Imaging Cellular Responses to Mechanical Stimuli Within Three-Dimensional Tissue Constructs

WEI TAN,[1] CLAUDIO VINEGONI,[1] JAMES J. NORMAN,[2] TEJAL A. DESAI,[2] AND STEPHEN A. BOPPART[1,3–5]*
[1]*Biophotonics Imaging Laboratory, Beckman Institute for Advanced Science and Technology, University of Illinois at Urbana-Champaign, Illinois*
[2]*Department of Biomedical Engineering, Boston University, Boston, Massachusetts*
[3]*Department of Electrical and Computer Engineering, University of Illinois at Urbana-Champaign, Urbana, Illinois*
[4]*Department of Bioengineering, University of Illinois at Urbana-Champaign, Urbana, Illinois*
[5]*Department of Internal Medicine, College of Medicine, University of Illinois at Urbana-Champaign, Urbana, Illinois*

KEY WORDS three-dimensional microscopy; optical coherence tomography; multi-photon microscopy; tissue engineering; scaffolds; cellular biomechanics

ABSTRACT The cellular response to environmental cues is complex, involving both structural and functional changes within the cell. Our understanding of this response is facilitated by microscopy techniques, but has been limited by our ability to image cell structure and function deep in highly-scattering tissues or 3D constructs. A novel multimodal microscopy technique that combines coherent and incoherent imaging for simultaneous visualization of structural and functional properties of cells and engineered tissues is demonstrated. This microscopic technique allows for the simultaneous acquisition of optical coherence microscopy and multiphoton microscopy data with particular emphasis for applications in cell biology and tissue engineering. The capability of this technique is shown using representative 3D cell and tissue engineering cultures consisting of primary fibroblasts from transgenic green fluorescent protein (GFP) mice and GFP-vinculin transfected fibroblasts. Imaging is performed following static and dynamic mechanically-stimulating culture conditions. The microscopy technique presented here reveals unique complementary data on the structure and function of cells and their adhesions and interactions with the surrounding microenvironment. *Microsc. Res. Tech. 70:000–000, 2007.* © 2007 Wiley-Liss, Inc.

INTRODUCTION

Microscopic techniques have been used to investigate the fundamental roles that mechanical forces and cell-material interactions play in cell culture and in the fields of cell biology, tumor biology, and tissue engineering. To maintain proper functionality, cells rely on adhesions to and interactions with the surrounding substrate, structure, or extracellular matrix. The surrounding microenvironment provides a construct in which cells move, orient, organize, and differentiate to form cultures and tissues. Mechanical forces transduced through the microenvironment also alter both the morphology and genetic expression patterns of the cells. Cell-material interactions are one of the key components in tissue engineering (Desai, 2000; Griffith, 2002). While the molecular bases of the cell–substrate interactions have been extensively studied, much less is understood about the dynamic response of cellular and subcellular structure to the microenvironment, especially for cells in artificial, 3D tissue-like constructs. One primary reason for this limited investigation is because of the inadequate imaging technology for high-resolution, real-time, noninvasive imaging deep within highly scattering tissues or tissue constructs. Furthermore, simultaneous 3D visualization of both cell morphology and material structures is problematic using current microscopic methods.

Conventional microscopy techniques at visible wavelengths such as light and fluorescence microscopy, though widely applied for imaging cellular and molecular activities, have disadvantages mainly because of poor light penetration depth in highly-scattering tissues, and the potential of severe photodamage to living cells. More advanced technologies for imaging engineered tissues, including high-field strength magnetic resonance imaging and microcomputed tomography, have been pursued for the assessment of cell or scaffold structure, with limited success. These techniques, with long data acquisition rates, hazards associated with high-energy radiation, and relatively high costs, are less suitable for both real-time and long-term imaging of living, dynamic, 3D cultures (Constantinidis et al., 2002; Lin et al., 2003).

Confocal microscopy has been an important advance in microscopy, and has enabled the imaging of intact, optically nontransparent specimens to produce high-resolution (submicron) images of tissue structure with the use of fluorescent probes (Breuls et al., 2003; Gareau et al., 2004; Stephens and Allen, 2003). For a thick

*Correspondence to: Stephen A. Boppart, M.D., Ph.D., Biophotonics Imaging Laboratory, Beckman Institute for Advanced Science and Technology, 405 N. Mathews Avenue, Urbana, IL 61801. E-mail: boppart@uiuc.edu

Received 7 September 2006; accepted in revised form 7 November 2006

Contract grant sponsor: National Institutes of Health; Contract grant number: 1 R01 EB00108; Contract grant sponsor: National Science Foundation; Contract grant number: BES 05-19920.

DOI 10.1002/jemt.20420

Published online in Wiley InterScience (www.interscience.wiley.com).

3D specimen (up to ~100 μm), confocal microscopy accomplishes optical sectioning by scanning the specimen with a focused beam of light and collecting the fluorescence signal via a pinhole aperture that spatially rejects light from out-of-focus areas of the specimen. Multiphoton microscopy (MPM), which relies on the simultaneous absorption of two or more near-infrared photons from a high-intensity short-pulse laser (most commonly a mode-locked titanium:sapphire laser) extends imaging depths to several hundreds of microns (Denk et al., 1990; Rubart, 2004). Longer-wavelength excitation light in MPM has the advantage of being scattered and absorbed less in biological tissue, resulting in this improved imaging depth, with little thermal damage. Exogenous fluorescent probes are usually required for detection in confocal microscopy or MPM, often limiting the long-term viability of the cells being imaged. Green fluorescent protein (GFP) and other genetically-expressible fluorescent proteins have been established as a powerful imaging method for long-term, in situ, dynamic imaging applications (Lippincott-Schwartz and Patterson, 2003; Tsien, 1998). Thus, the two-photon GFP imaging method is one component in our multimodal imaging studies of cells and adhesion proteins, used as a means of recognizing functional changes in cells.

Optical coherence tomography (OCT) has been demonstrated as a noninvasive and high-resolution imaging technique for locating and diagnosing pathological tissue by generating cross-sectional images that approach the resolution and appearance of histology (Huang et al., 1991). However, only the linear characteristics of the tissue, such as scattering, birefringence, absorption, and refractive index variations contribute to producing image contrast. Optical coherence microscopy (OCM) (Izatt et al., 1994) extends the capabilities of OCT by combining high sensitivity and coherence-gated detection with confocal optical sectioning. The result is an improvement in the rejection of unwanted scattered light generated from points outside of the imaging plane (Aguirre et al., 2003). A dramatic enhancement of the image contrast is therefore possible, at greater imaging depths in highly-scattering tissue. OCT does not rely on the use of exogenous agents or genetically-expressed fluorescent proteins to provide image contrast, but rather the intrinsic optical scattering (indices of refraction) differences in cells and tissues. Because of this, OCT can be performed repeatedly over long periods of time with no loss of cell viability.

Recently, alternative approaches have been proposed that combine different optical imaging techniques to provide different yet complementary information (Barton et al., 2004; Beaurepaire et al., 1999; Dunkers et al., 2003; Tang et al., 2006). MPM and OCM are two emerging imaging techniques that both utilize near-infrared wavelength light to enable deep-tissue imaging. OCM, which can be performed without the use of contrast agents, is a coherent-detection technique that generates structural images based on optical backscatter, or local variations in the refractive index. MPM, using fluorescently labeled molecules or genetically-expressed proteins, is an incoherent functional imaging technique, where the expression of fluorescent proteins can be designed to correspond to functional physiological parameters within the cell. The multimodal microscopy technique presented here uniquely enables the identification of functionally-active signals against a comprehensive background of scattering signals representative of the structural microenvironment around specific cells or small populations of cells. In this context, we wish to apply this technique to visualize functional changes in cells on various substrates, in 3D scaffolds, and under static and dynamic culture conditions.

We have developed this visualization technique using a custom-built integrated microscope (Vinegoni et al., 2006) that can perform simultaneously OCM and MPM with the same ultrafast titanium:sapphire laser source. The imaging results presented here are representative of cell structure and functional adhesion data from 2D planar and topographic culture substrates, and from 3D engineered tissue scaffolds. The use of spectral-domain OCM not only provides structural information of the substrate (e.g., micropeg structure) or the extracellular matrix (e.g., microfibers), but also shows cell morphology. Simultaneously, MPM offers complementary information on cell adhesions as well as subcellular structures. Using this approach, we find and map the spatiotemporal distribution of GFP within cells, which varies under static and dynamic culture conditions. This novel 3D imaging technique enables us to better understand and visualize the biological, chemical, mechanical, and materials effects on the cellular scale, how these affect the cellular physiology and response to chemical and mechanical stimuli, and how to design suitable micro-environments for cells in 3D scaffolds.

MATERIALS AND METHODS

Multimodality Microscope

The setup of the microscope used in this work is shown in Figure 1. The light source consists of a frequency-doubled Nd:YVO_4-pumped titanium:sapphire laser with a center wavelength of 800 nm, a bandwidth of 60 nm, an 80 MHz pulse repetition rate, and an average power on the sample that can be varied between 1 and 10 mW. The laser source serves both as an excitation source for two-photon fluorescence and as a low-coherence source for OCM, facilitating the multimodality imaging capabilities of this microscope. Because of the highly dispersive nature of the microscope objective (20×, 0.9 NA, water-immersion, Olympus), the pulses are precompensated using a doublefold prism path. The beam is directed to a scan head that consists of two galvanometer-controlled mirrors for high-speed acquisition, and then beam expanded to match the back-aperture of the objective in this upright microscope configuration. Samples were fixed on a holder attached to a 3D translation stage. The photons resulting from the two-photon absorption process are emitted over the entire 4π solid angle. A portion of the signal is collected in the backward direction by the objective and deflected by a dichroic beam-splitting mirror (Cold Mirror, CVILaser, Livermore, CA). The photons are then collected and coupled into a multi-mode fiber. A short pass filter (BG39, CVILaser) located prior to the fiber is used to filter out scattered pump photons. The filter can be easily interchanged for use with different selected fluorophores or for second-harmonicgeneration imaging. A photomultiplier tube (H7421-40,

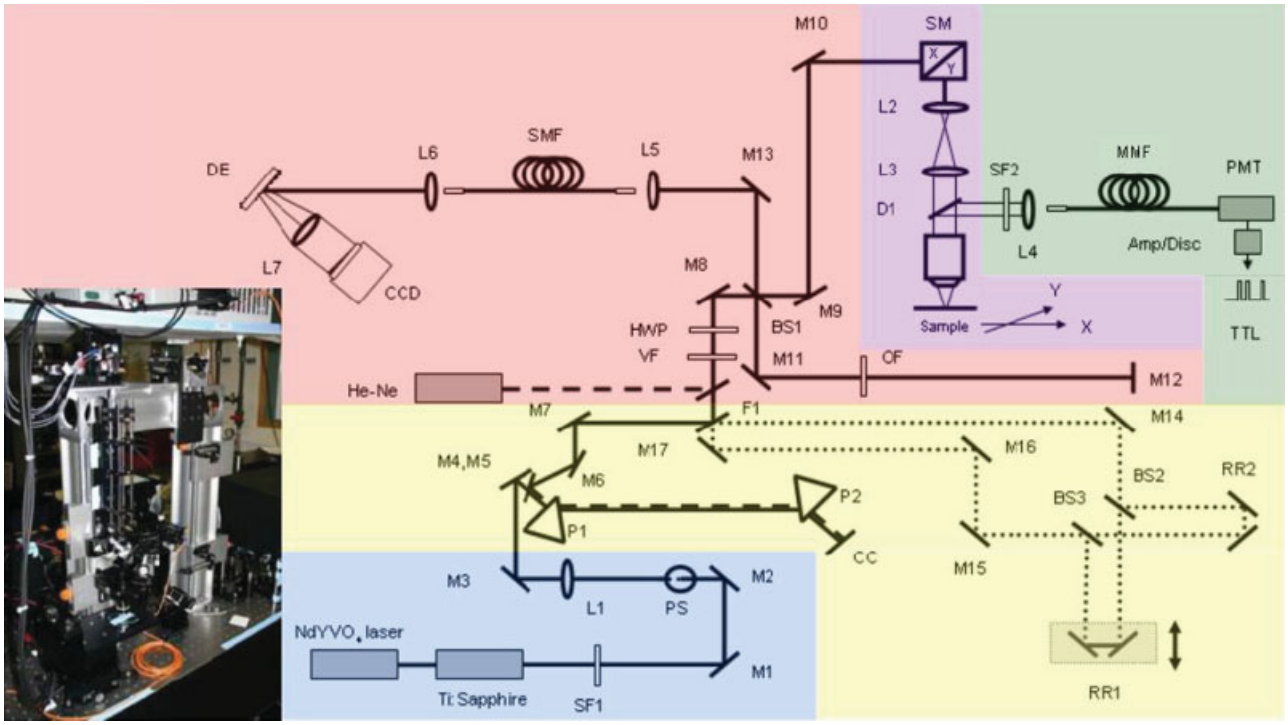

Fig. 1. Experimental setup for the multimodality microscope. Colored regions correspond to: blue-optical source, red-OCM, green-MPM, yellow-dispersion compensation, purple-main optical axis of the microscope. Inset shows the optical hardware for the upright microscope configuration corresponding to the purple-colored region in the schematic. Abbreviations: Amp/Disc, amplifier/discriminator; BS, beam splitter; CC, corner cube; CCD, charge-coupled device (line scan camera); D, dichroic beam-splitter; DE, diffraction grating; He–Ne, helium-neon alignment laser; HWP, half-wave plate; L, lens; M, mirror; MMF, multimode fiber; OF, optical neutral density filter; P, prism; PMT, photomultiplier tube; RR, retroreflector; SF, spatial filter; SM, scanning mirrors; SMF, single-mode fiber; TTL, photon-counting signal; VF, variable filter. [Color figure can be viewed in the online issue, which is available at www.interscience.wiley.com.]

Hamamatsu, Inc.) working in photon counting mode was used to detect two-photon fluorescence, with a maximum quantum efficiency of 30% at 580 nm, and a dark counts rate of 100 Hz. When overfilling the back-aperture (18 mm) of the objective, axial and lateral two-photon resolutions of 0.8 and 0.5 μm, respectively, were measured.

The OCM detection scheme in this integrated microscope is different with respect to a previously reported system (Beaurepaire et al., 1999). A spectral-domain OCM (SD–OCM) system, instead of time-domain OCM is implemented, offering many distinct advantages (Leitgeb et al., 2003). Light is collimated and dispersed off of a blazed diffraction grating having 830.3 grooves/mm. The optical spectrum is focused using a pair of achromatic lenses which have a combined focal length of 150 mm. The focused light is incident on a line-scan camera (L104k–2k, Basler, Inc.) that contains a 2048-element CCD array of detection elements. This camera has a maximum readout rate of 29 kHz, thus one axial scan (corresponding to one pixel in an *en face* optical section) can be captured during an exposure interval of 34 μs (temporal resolution). Digital processing of the detected signal included a spline interpolation to make the signal more uniform, and a discrete Fourier transform on each set of 2048, 10-bit, values captured by the CCD to transform the signal from the frequency (spectral) domain into the spatial (depth) domain. The scattering amplitudes corresponding to the focus in each adjacent axial scan were subsequently assembled into 2D *en face* images for visualization on a personal computer. To produce 3D volume images, the sample position was stepped in the axial (depth) direction using a precision computer-controlled stage and repeated 2D *en face* images were acquired and assembled. Acquisition and visualization of OCM and MPM images was performed simultaneously. In our system, the confocal gating (confocal parameter and OCM axial resolution at 2.2 μm) is below the coherence gating (coherence length = 4.7 μm) with the laser source bandwidth of 60 nm. The bandwidth of this laser source could be increased, with concomitant dispersion compensation, to effectively improve the axial OCM resolution. The addition of coherence gating to confocal gating further rejects out-of-plane photons by adding coherent rejection to the spatial rejection and enabling deeper imaging penetration. By use of the edge-scan definition, a transverse resolution of less than 0.9 μm was measured.

Cell Culture and Experimental Conditions

Two types of cells were used in our investigations: primary muscle fibroblasts derived from transgenic GFP mice, and 3T3 fibroblasts (American Type Culture Collection [ATCC], Manassas, VA) transfected with GFP-vinculin plasmid. Cells were also stained with a nuclear dye (Hoechst 33342, Invitrogen). Cell cultures were seeded using 5×10^5 cells/mL and maintained in

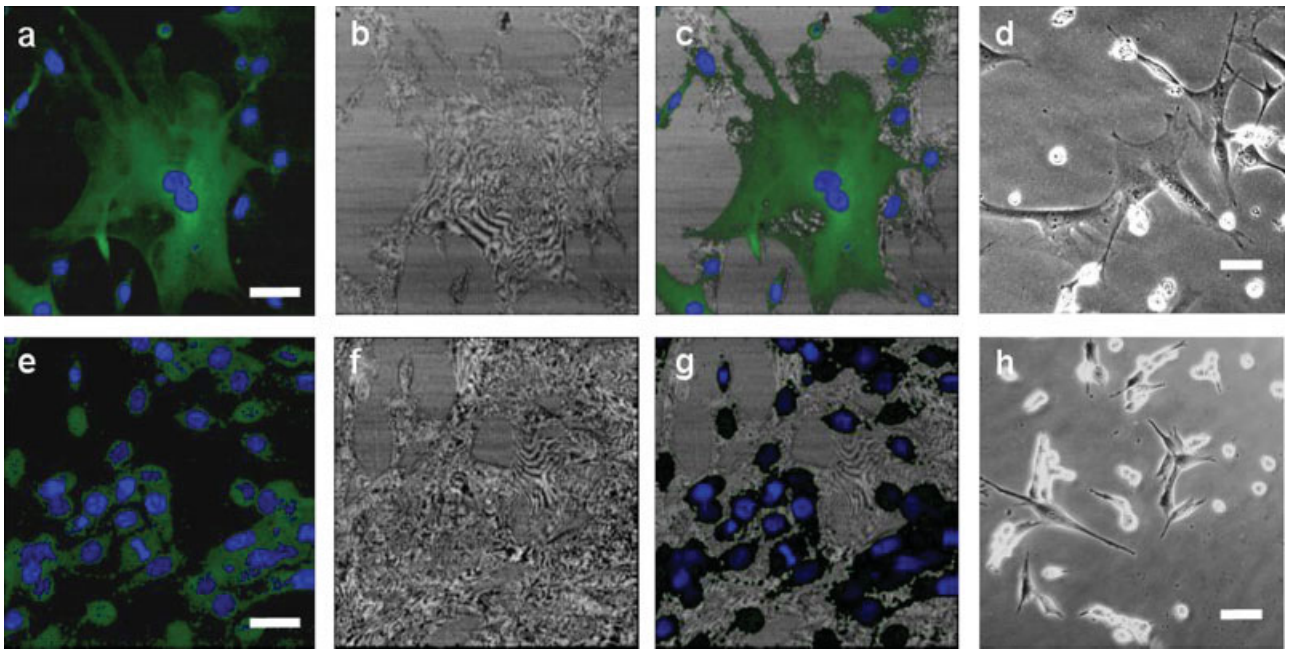

Fig. 2. Multimodal microscopy of fibroblasts on a planar substrate. (**a**–**d**) Fibroblasts from a GFP-mouse, and (**e**–**h**) 3T3 fibroblasts with GFP-vinculin are imaged in this 2D culture. (a, e) MPM and (b, f) OCM image channels are combined (c, g) for multimodal visualization to demonstrate the relationship between cell morphology, cell adhesion activity, and nuclei (blue channel). (d, h) Phase contrast microscopy of similar cultures is shown for comparison. The light-dark banding observed in (b, f) is due coherent interference effects from reflections off of the planar substrate and the cell membrane. Scale bars = 20 μm. [Color figure can be viewed in the online issue, which is available at www.interscience.wiley.com.]

an incubator at 37°C and with 5% CO_2. Different cell and engineered tissue cultures are employed in the study. These include cells cultured in planar Petri dishes, on flexible microtextured poly(dimethyl-siloxane) (PDMS) substrates with 3D topographic features (micropegs), and in 3D Matrigel (BD Bioscience) polymer scaffolds. Cultures on flexible PDMS and in Matrigel were maintained under static and mechanically-stimulating conditions. Mechanical stimulation of cultures began following 3 days of static culture conditions to enable cells time to establish cell–cell and cell–matrix interactions and adhesions. The microtextured substrates were fabricated with soft lithography methods, generating the structures first on a silicon substrate using photolithography methods, and then transferring the patterns to PDMS membranes. The mechanical stimulation system, consisting of both a TissueTrain and a StageFlexer system (Flexcercell, NC), was used to stimulate cells on the microtextured PDMS or cells in the 3D Matrigel. Cells mechanically stimulated with the TissueTrain system were subjected to equibiaxial cyclic stretching, while cells mechanically stimulated with the StageFlexer system were subjected to uniaxial cyclic stretching.

Image Visualization and Three-Dimensional Reconstruction

Acquired images (OCM, MPM) typically consisted of 1,000 × 1,000 pixels over an area of 600 × 600 μm^2. OCM and MPM signals were acquired simultaneously for each point in the image as the focused beam was raster-scanned across the sample, permitting precise registration between imaging modalities. A precision *z*-axis (depth) computer-controlled translation stage allowed for the acquisition of stacks of *en face* OCM and MPM images. Three-dimensional visualization of the engineered tissue constructs was achieved by volume rendering the image stacks of OCM and MPM data using 3D reconstruction software (Analyze 5.0, Mayo Clinic, Rochester, MN).

RESULTS

A custom-designed and constructed multi-modality microscope (Fig. 1) was used in this study (Vinegoni et al., 2006). This instrument provides noninvasive imaging capabilities to detect high-resolution 3D structural and functional information. This information is essential for the applications that involve both biological and nonbiological microscopic elements, such as cells and materials in tissue engineering constructs. Shown in Figure 2, this multimodality technique provides high resolution image data of cell morphology, nuclei, and intracellular adhesion molecules. Primary muscle fibroblasts obtained from a transgenic GFP mouse, as well as a 3T3 fibroblast cell line transfected with GFP-vinculin genes were used to demonstrate this technique and capabilities. Cells are clearly visible in the images from OCM (Figs. 2b and 2f). In fact, interference bands are present over some cell locations, representing interference of the coherent backreflected light from the surfaces of the substrate and the cell membrane. The interference fringe data could be used to measure cell thickness and structural changes with nanometer resolution. The OCM images of cells look similar to those from standard phase-contrast microscopy (Figs. 2d and 2h). OCM, however, can provide

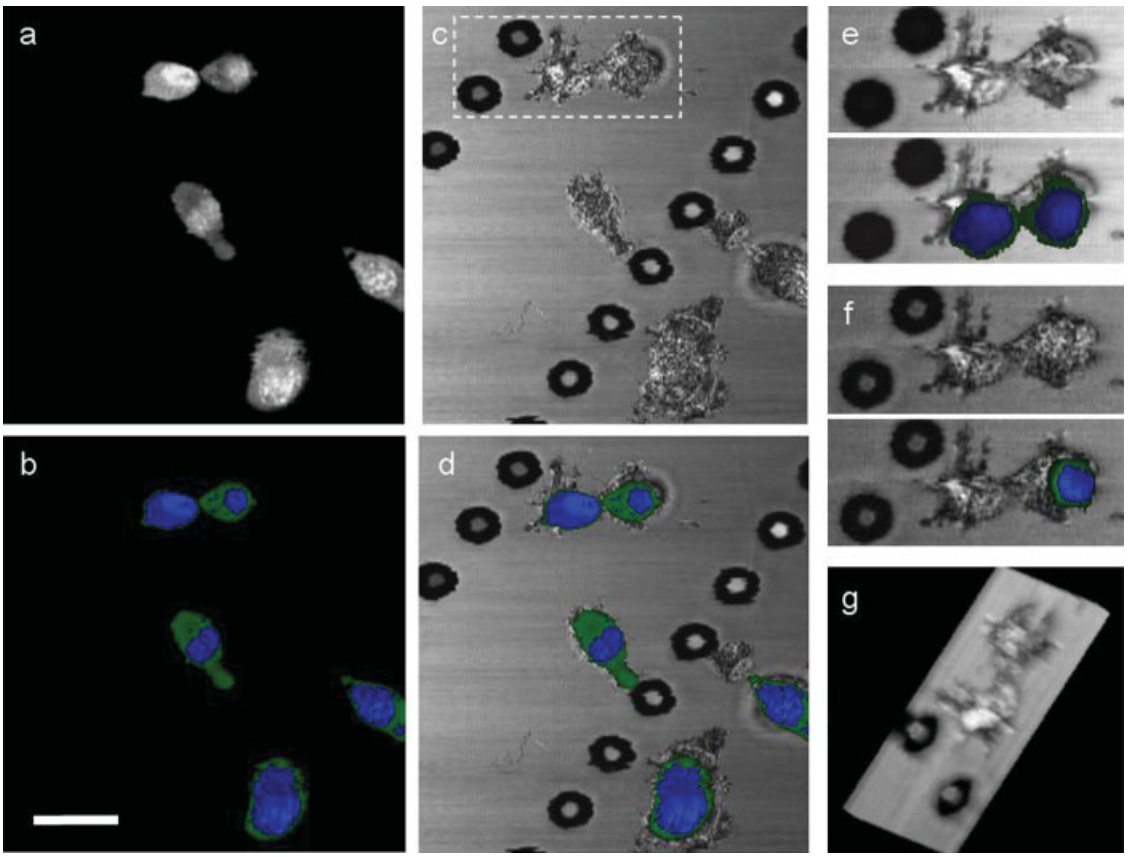

Fig. 3. Functional interactions between GFP-vinculin fibroblasts and a microtextured (micropeg) substrate. Images were acquired under static culture conditions. (**a**) Combined and (**b**) separated MPM signals. The green channel represents fluorescence from GFP-vinculin and is proportional to the degree of cell adhesions with other cells and the substrate. (**c**) OCM image showing backscattering signal from both cells and microtextured substrate. (**d**) Multimodal image of MPM and OCM data showing distinct spatial relationships between cells and substrate features. (**e**, **f**) Regions of OCM and combined OCM-MPM data indicated by box in (c) but acquired at different *en face* planes 6 μm and 12 μm, respectively, above the plane in (c). (**g**) 3D reconstruction of OCM data set showing cellular morphology on the substrate. Scale bar = 20 μm. [Color figure can be viewed in the online issue, which is available at www.interscience.wiley.com.]

reflectance-based imaging deep in highly-scattering tissues, which is problematic in phase microscopy. Cell morphology in OCM images (Figs. 2b and 2f) correspond strongly with that observed in MPM images (Figs. 2a and 2e). The spatial distribution of fluorescence intensity in the cells varies in the MPM images, corresponding to the relative concentrations of fluorescing molecules. The OCM backscatter signal intensity also varies in the cells. In addition to the interference banding, this varying backscatter signal may be correlated with subcellular structures (Xu et al., 2006).

Though the two imaging modalities are adapted for simultaneous imaging, the resolutions of the two modalities are different. The MPM *en face* sections are thinner (~0.5 μm), offering higher resolution in the z (depth) dimension compared to the OCM images, which has ~2.2 μm resolution in the z dimension. The axial resolution in MPM is defined by the region of two-photon absorption of incident photons, which has a quadratic dependence on the laser intensity. The axial resolution in OCM, in these studies, was primarily dependent on the confocal parameter of the focusing objective. This is in contrast to cross-sectional OCT imaging where the axial resolution is defined by the coherence length of the light source, which is inversely dependent on the bandwidth of the light. OCT utilizes lower numerical aperture objectives and hence, the coherence length is typically smaller than the confocal parameter of the focusing lens. The combination of coherence gating within the confocal parameter of the focused beam further rejects out-of-focus photons and is what enables OCM to be performed to greater depths in highly-scattering tissues than with confocal microscopy alone (Izatt et al., 1994). Imaging depths are highly dependent on the tissue construct composition, cell types, and density, and culture conditions. In general, from our studies, maximum imaging depths for OCM and MPM were ~1,000 and 500 μm, respectively, for these constructs. An optical attenuation coefficient of 1.24 cm^{-1} was measured for the cell-free Matrigel constructs at 768 nm wavelength.

Using GFP-vinculin-labeled adhesion sites and Hoechst-stained nuclei, the combined OCM–MPM images (Figs. 2c and 2g) demonstrate the relative spatial distributions of these signals within individual cells and among these cell populations. Vinculin is an abundant cytoskeletal protein found in integrin-mediated focal adhesions and also in cadherin-mediated cell–cell adherens junctions. Vinculin expression there-

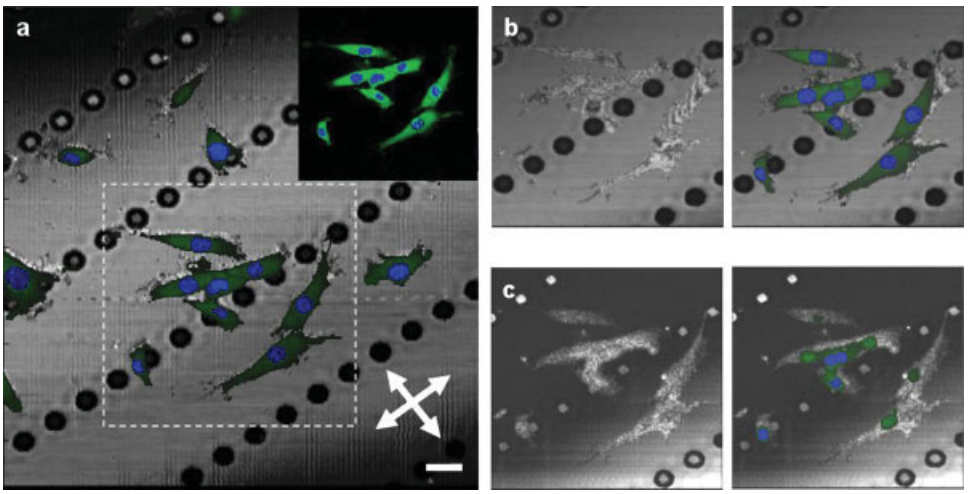

Fig. 4. Functional interactions between GFP-vinculin fibroblasts and microtextured substrate following mechanical stretching of the elastic polymer substrate. Substrate was subjected to 18 h of 5% cyclic equibiaxial sinusoidal stretching at a frequency of 1 Hz and in the directions indicated by the arrows. (**a**) Multimodal image combining OCM and MPM data. Inset shows the MPM channel. (**b**, **c**) OCM and multimodal images of boxed region in (a) at *en face* planes 6 μm and 12 μm, respectively, above the plane in (a). Note the increase in GFP-vinculin signal-expression, which is present over a larger area of the cells. The images in (c) illustrate the depth-dependent optical sectioning of this instrument. At this plane, signal from the planar substrate is decreased (darker), while the upper peg surface reflection is increased. MPM signals from the cells are decreased at the upper *en face* imaging planes of these cells. Scale bar = 20 μm. [Color figure can be viewed in the online issue, which is available at www.interscience.wiley.com.]

fore reflects the degree of cell–cell and cell–substrate adhesions in these cultures. The most significant advantage of this method is the ability to extract new information regarding the spatiotemporal distribution of functionally-active fluorescent signals (adhesions in this context) against a background of scattering signals coming from all structures present. It is clear from the combined OCM-MPM images that the fluorescent signals are generated from only portions of the cell, where cell–cell or cell–substrate adhesions are present and where GFP-vinculin is expressed. This method therefore allows the characterization of focally-active adhesion sites and provides spatial and temporal variations of cell function. While these studies utilize transfected GFP-vinculin as the functionally-active and expressed fluorescent protein, it is feasible to use any of the increasingly common genetically-expressed fluorescent proteins for visualizing cellular function or even single-molecule dynamics against the OCM reflectance background from the microenvironment.

In addition to image data of cell morphology, microstructural data of scaffolds, and cell-scaffold interactions can be readily obtained using this method. The reliance of scattering signals from the scaffolds or structures obviates the need to fluorescently label all structures (biological and nonbiological) for visualization. To demonstrate this capability, microtextured polydimethyl-siloxane (PDMS) membranes were used. The microtextured substrate consisted of rows of 10 μm high and 10 μm diameter micropegs, separated by 50 μm between rows (Figs. 3 and 4). Biophysical stimuli provided through surface textures (surface topographies) have been reported to influence cell shape, gene expression, protein production, and deposition, cell proliferation, migration, differentiation, and survival (Curtis and Riehle, 2001; Stevens and George, 2005). Therefore, exploring the effects of microscale textures at the cell–cell and cell–scaffold interface provides an attractive approach to enhance cell behavior without destabilizing the delicate biochemical condition.

The OCM images in Figure 3 demonstrate the structural information of the cells, the substrate, and the spatial arrangement. The MPM images reveal the locations of the nuclei and the expression of the GFP-labeled vinculin. The cells tend to spread and extend around the microscale 3D structural features. Vinculin expression is more extensive at the sites where cell–cell or cell–substrate interactions are occurring. Thus, the combined OCM–MPM images provide complementary and additive information regarding the cells in relation to the local environment, and in this representative example, the functional adhesion behavior of the cells. Compared to cells cultured on planar, featureless Petri dishes or slides, cells cultured on microtextured and topographic substrates display more 3D culture characteristics (Norman and Desai, 2005). Using this imaging technique, we have also demonstrated the 3D changes of intracellular structural and functional sites over the volume of the cells (Figs. 3e and 3f), and have reconstructed a series of *en face* OCM images to produce a 3D image of cell structure (Fig. 3g).

Complementary structural and functional information of cell dynamics (e.g., cell–cell and cell–scaffold interactions) under mechanically-stimulated culture conditions has also been obtained. The representative images of fibroblasts after 18 h of 5% cyclic equibiaxial sinusoidal stretching at a frequency of 1 Hz are shown in Figure 4. Compared to the cells on these microtextured substrates before mechanical stretching (Fig. 3), the cells subjected to mechanical stimuli are more elongated, have a higher level of vinculin expression based on the intensity and distribution of fluorescence from the GFP-vinculin, and have an apparent increase in cell-substrate interactions.

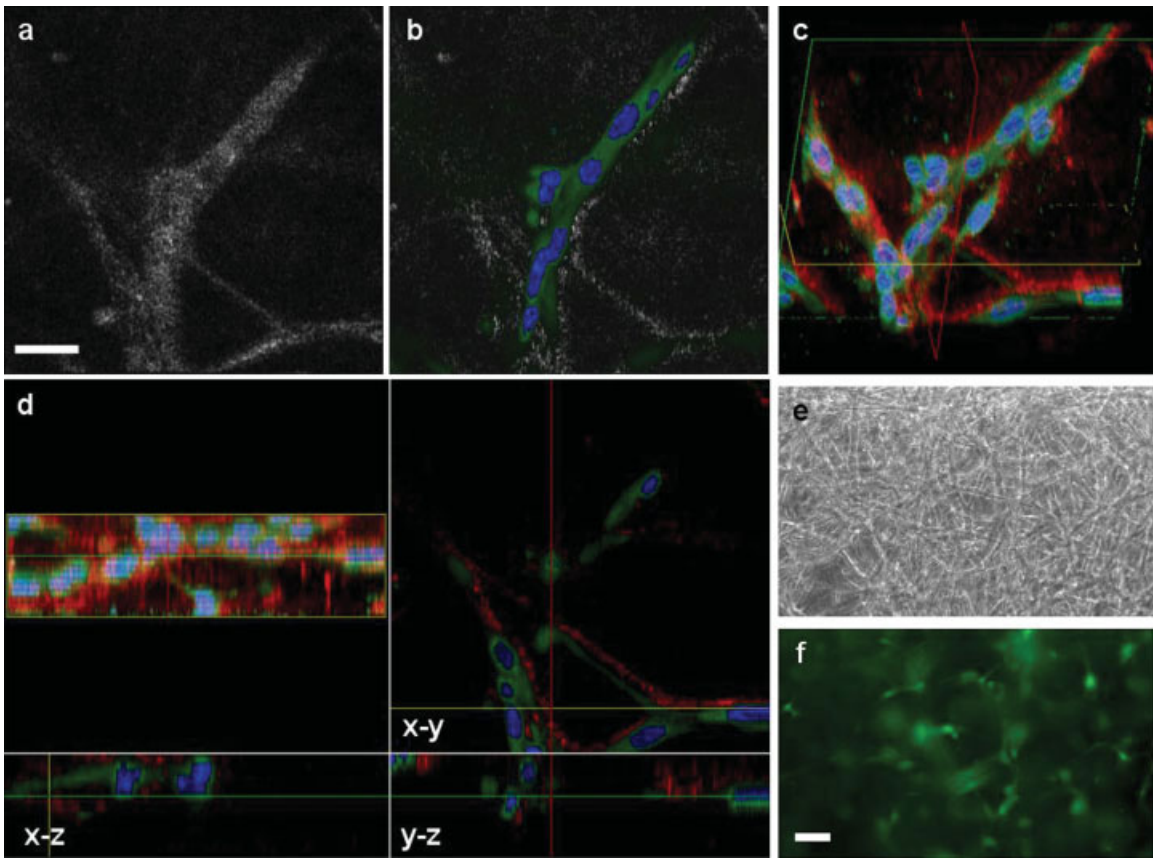

Fig. 5. Three-dimensional multimodal images of fibroblasts from a transgenic GFP mouse cultured in a Matrigel scaffold. Culture was maintained and imaged under static conditions. (**a**) OCM, (**b**) multimodal, and (**c**) 3D multimodal images of cells in this 3D tissue construct. (**d**) Projections in the *x–y*, *x–z*, and *y–z* planes are shown for the 3D data. Color channels correspond to: Gray or Red- OCM, Blue- nuclei, Green– GFP. (**e**) Phase-contrast and (**f**) fluorescence microscopy images of the same 3D cultures are shown for comparison. Scale bars = 20 μm.

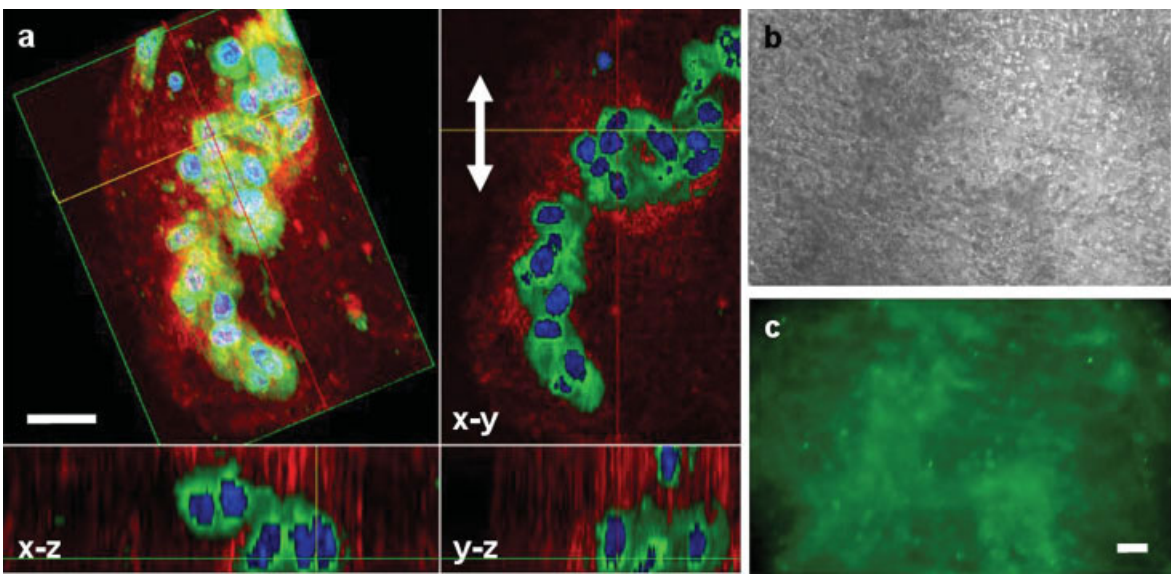

Fig. 6. Three-dimensional multimodal images of fibroblasts from a transgenic GFP mouse cultured in Matrigel under mechanical stimulation. 3D culture was subjected to 18 h of 5% cyclic uniaxial sinusoidal stretching at a frequency of 1 Hz and in the directions indicated by the arrows. (**a**) 3D multimodal images of cells, with corresponding projections in three orthogonal planes. Color channels correspond to: Red – OCM, Blue – nuclei, Green – GFP. (**b**) Phase-contrast and (**c**) fluorescence microscopy images of the same 3D cultures are shown for comparison. Scale bars = 20 μm.

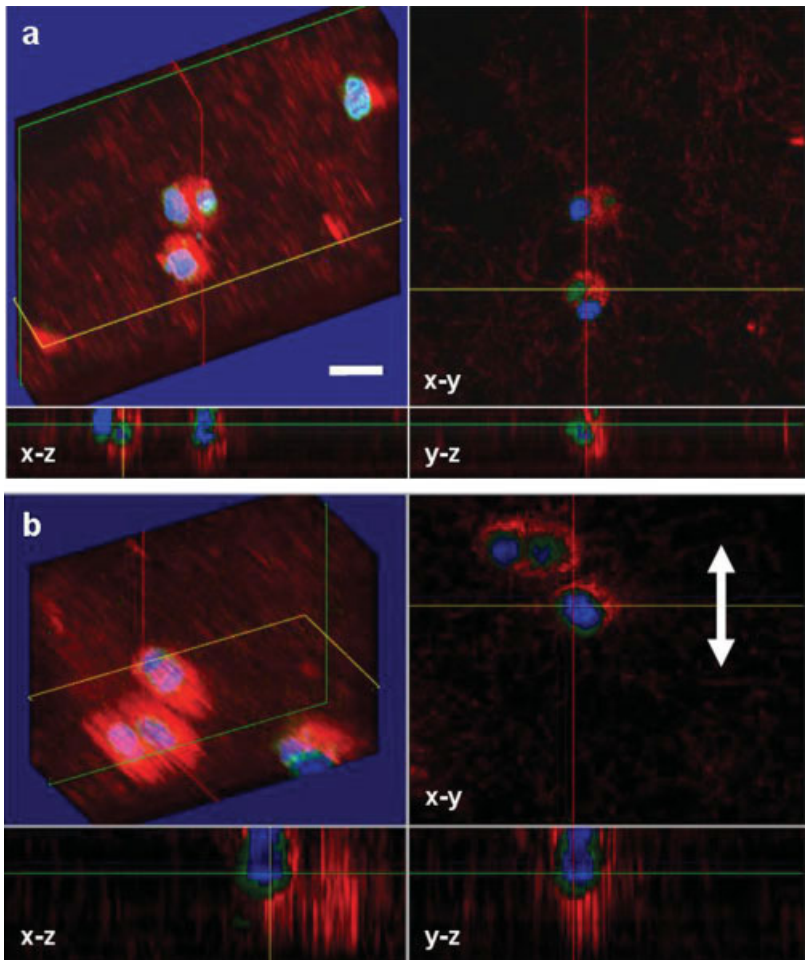

Fig. 7. Three-dimensional multimodal images of GFP-vinculin fibroblasts. Cells were seeded in a 3D Matrigel scaffold and cultured under (**a**) static and (**b**) dynamic conditions. The 3D scaffold with cells in (b) was subjected to 18 h of 5% cyclic biaxial sinusoidal stretching at a frequency of 1 Hz and in the directions indicated by the arrows. Note the distinct differences in cell morphology and GFP-vinculin expression, both before and after mechanical stimulation, compared to the primary cells in Figure 6. Spherical cell morphology and decreased GFP-vinculin expression is likely due to reduced number of cell adhesions within the Matrigel matrix. Scale bar = 20 μm. [Color figure can be viewed in the online issue, which is available at www.interscience.wiley.com.]

A further application of this technique involves the use of this instrument to dynamically study cell-scaffold interactions under more physiological 3D culture conditions, as shown in Figures 5–7. This multimodality technique provides the capability for noninvasive imaging at the molecular, cellular, and tissue levels in 3D. The two types of fibroblast cells described above were cultured in a 3D Matrigel matrix. The OCM images show the 3D cell morphologies and positions as well as the background fibrous matrix structure and network. The MPM images track nuclei and focal adhesion sites in the cells. Figures 5 and 6 demonstrate the primary GFP-mouse fibroblasts cultured in Matrigel under static conditions (Fig. 5) and after 18 h of 5% cyclic uniaxial sinusoidal mechanical stretching at a frequency of 1 Hz (Fig. 6). It is believed that the mechanical deformation of the biopolymer fibers to which cells attach induces alterations in cell morphology, physiology, and gene expression. The cells cultured under static conditions exhibit elongated morphology and 3D network structure. Cells are oriented and extend isotropically in 3D space, following the random orientation of the matrix structure. After uniaxial mechanical stretching, the cells and matrices are densely packed and align parallel with the stretched axial direction.

Figure 7 demonstrates the GFP-vinculin-labeled 3T3 fibroblasts cultured in 3D Matrigel under static conditions (Fig. 7a) and after 18 h of 5% cyclic biaxial sinusoidal mechanical stretching at a frequency of 1 Hz (Fig. 7b). This cell line in Matrigel exhibits fewer focal adhesion sites than the primary fibroblasts. Compared to the elongated oval-shaped fibroblasts cultured in 2D planar and 3D topographic cell culture (Figs. 2, 3, and 4), these cells in 3D Matrigel display a spherical morphology with spherical nuclei and minimal vinculin expression. This might be due to the lack of certain transmembrane protein receptors to the Matrigel protein sequences. Matrigel is mainly composed of laminin and collagen IV and lacks many of the proteins associated with cell adhesions, such as collagen I and fibronectin. Vinculin is not highly expressed under these conditions and thus adhesions and interactions between the cells and the Matrigel is less, as evidence by the significantly reduced fluorescence from the GFP-labeled vinculin. It is also noted that cell morphology and vinculin expression in this 3D culture do not change significantly after mechanical stretching (Fig. 7), which is also likely attributed to matrix composition. These results may also suggest some functional characteristics of these immortal cell lines are down-regulated.

DISCUSSION

Three-dimensional visualization of cell structure and function is essential for investigating the dynamics of cells in natural or artificial microenvironments. While phase-contrast microscopy is a powerful tool for the visualization of unstained biological specimens, it cannot be used for 3D visualization deep in highly-scattering tissues. OCM demonstrated here offers a new approach to 3D visualization of optical contrast in unstained samples. The optical contrast in cells detected by OCM arises primarily from scattering because of spatial refractive-index gradients and geometric sizes of cellular components. Many functional imaging applications of unstained cells require quantification of subtle phase-contrast changes in a cell with subcellular resolution. Although it has not been shown in these results, the subcellular structure may be identified using a method called spectroscopic OCM (SOCM). Scattering-based spectroscopic analysis of the OCM or OCT signal can be used to identify subcellular structures such as nuclei. Spectroscopic OCT, a recent extension of OCT imaging, analyzes not only the intensities, but also the spectra of back-scattered light in a depth-resolved manner (Leitgeb et al., 2000; Morgner et al., 2000). This technique is capable of both qualitative contrast enhancement and quantitative concentration measurement (Xu et al., 2004). Spectroscopic analysis of spectral-domain OCM measurements, in combination with high sensitivity intensity measurements afforded by traditional OCM, offers a potentially powerful tool for adding functional information to the structural information, e.g., localizing dominant scatterers such as nuclei (Xu et al., 2006). Because of the multimodality capabilities of this instrument, the findings of these subcellular structures using SOCM can be further confirmed with labeling techniques and MPM imaging, as was done with the DNA/nuclei co-staining in these experiments. Thus, further efforts on correlating the SOCM analysis of the resulting images with MPM imaging and molecular staining will give more insight into the cell–cell and cell–substrate interactions from this study.

Our approach for using spectral-domain detection of the OCM signal was motivated by several advantages over previous time-domain techniques. Spectral-domain OCT, in previous studies (Leitgeb et al., 2003), has been shown to offer a significant improvement in signal-to-noise over time-domain OCT, with similar advantages in OCM. In addition, because no moving parts are required for collecting axial-scan data using spectral-domain (spectrometer-based) detection, the phase measurements of the backscattered light are extremely stable, facilitating spectroscopic analysis of the spectral data, which is directly captured on the line-scan camera. Because a full axial-depth scan of scattering and spectroscopic data is collected at each point in an *en face* image, this data can be used for both high spatial and high spectral resolution imaging. The ability to perform focus tracking to accommodate for varying refractive indices in the sample is facilitated in our approach since multiple points in depth are acquired and available for reconstruction. The use of spectral-domain detection in OCM does result in longer acquisition times compared to time-domain OCM where only the amplitude (scattering) data is collected. However, we believe the additional time required to collect and analyze spectroscopic data, as well as the phase-stability of these signals, enables a wider range of investigative techniques.

In these studies, PDMS was used for fabricating 3D topographic scaffolds and Matrigel was used for 3D polymer scaffolds. Both provided flexible constructs during mechanical stimulation of the cell cultures. Differences in cell morphology under static and mechanically-stimulated culture conditions were noted for the cultures on the 3D topographic PDMS scaffolds versus in the 3D Matrigel scaffolds. On the topographic PDMS scaffolds, fibroblasts had a more spherical morphology under static conditions (Fig. 3) and a more spindle morphology under mechanically-stimulated conditions (Fig. 4). This is in contrast to and opposite of the morphological changes for the fibroblasts in the 3D Matrigel scaffolds (Figs. 5 and 6). We believe these differences are attributable to the different microenvironments provided by each construct. In Figures 5 and 6, there is a higher local cell density and possibly an increase in contact and cell–cell interactions. Because the 3D cellular microenvironment on the topographic PDMS substrates differ significantly from the Matrigel scaffolds, it is likely that the cells experienced very different mechanical strain patterns, being more planar on the topographic PDMS substrates and more 3D in the Matrigel scaffolds. Future studies will explore other construct microenvironments and how these affect cell morphology under static and dynamic conditions.

Results indicative of specific cell-scaffold interactions were also found in Figure 7. The use of Matrigel, which lacks collagen I, was likely a contributing factor in the reduced amount of cell-scaffold adhesions and subsequently, the reduced GFP-vinculin expression. Matrigel was used as a 3D polymer scaffold in this study not only to illustrate the different functional behavior in these cells, but also because we have found this material to be optically superior to other scaffold materials. In a recent study (Tan et al., 2006), it was observed that when increasing amounts of collagen I were added to Matrigel constructs, the overall scattering of the construct increased, resulting in a reduced OCT imaging depth and reduced optical scattering contrast between cells and the surrounding matrix. Ongoing studies are characterizing the optical properties of various construct materials alone, with cells, and under varying culture conditions.

The last decade has seen dramatic developments of engineered tissues assembled from cells, biomaterials, and signaling factors. However, few have investigated the dynamics of biological interactions among these components at multiple size scales. The primary limitation has been inadequate imaging technology for high-resolution, real-time, noninvasive imaging deep within highly-scattering tissues. Compared with conventional invasive, destructive imaging techniques such as histology and SEM, OCM, and MPM are nondestructive, real-time, time-lapse imaging techniques that reveal essential cell and tissue characteristics. The elimination of specimen fixation and extensive processing reduces the possibility of structural artifacts and facilitates repeated observations within a single sample over time, and in response to various internal and external chemical and mechanical stimuli.

Furthermore, there is minimal disturbance to the cell and tissue physiology of the living samples because the laser power used to acquire images is low, the imaging speed is fast, requiring only a few seconds to acquire images, and living samples can be imaged in a sterile microincubator under physiological conditions as demonstrated in our previous work with an OCT system (Tan et al., 2004). In addition, both coherent (OCM) and incoherent (MPM) modalities can provide real 3D image information, which conventional invasive methods cannot provide.

This multimodality imaging technique, utilizing a single instrument, enables a wide range of biological investigations, with MPM based on the detection of the fluorescence emitted by endogenous or exogenous markers, and OCM delivering information on the endogenous scattering properties of the sample. These two modalities, therefore, provide different yet complementary imaging contrast mechanisms, increasing the information extracted from the sample. By overlaying the site-specific functional images from MPM (i.e., an excited fluorescent marker implies a functional protein) on the background structural image obtained from OCM, a more comprehensive view of different tissues can be obtained. Without any modification, this instrument can also be used to perform laser ablation, where the absorption is still a two-photon process but at much higher energies. This feature could be very useful in order to perform high resolution optical ablation followed by optical histology obtained by OCM for basic investigative studies in cell and tissue responses, as well as for medical applications.

With deep imaging penetration and high spatiotemporal resolution in 3D space, this novel imaging technique will be a potential tool for gaining new insights into cell dynamics in situ and in real-time, elucidating the complex biological interactions, and directing our design towards functional, biomimetic and matured engineered tissues. In addition, the potential for examining the structural features and interactions of cells and their 3D microenvironment represents a novel method for understanding the fundamental mechanisms of cell and tumor biology that are directly relevant for addressing many clinical questions.

In conclusion, we have developed a novel technique for interrogating the spatiotemporal relationship of structure and function of cells in 3D culture environments and in response to mechanical stimuli. This method is made possible with a novel multimodal microscope that is capable of simultaneous image acquisition of coherent and incoherent optical signals from biological specimens. This technique not only enables imaging at the molecular, cellular, and tissue level, but also facilitates and combines structural and functional imaging information that will likely contribute to many biological and clinical investigations.

ACKNOWLEDGMENTS

We wish to thank Drs. Daniel Marks and Amy Oldenburg from the Biophotonics Imaging Laboratory at the Beckman Institute for Advanced Science and Technology, University of Illinois at Urbana-Champaign, for their assistance in operating and maintaining the laser systems in our laboratory. Dr. Wei Tan is currently with the Department of Mechanical Engineering, University of Colorado at Boulder. Dr. Claudio Vinegoni is currently with the Center for Molecular Imaging Research, Massachusetts General Hospital, Harvard University. Dr. Tejal Desai is currently with the Departments of Physiology and Bioengineering, University of California – San Francisco. Additional information can be obtained at: http://biophotonics.uiuc.edu.

REFERENCES

Aguirre AD, Hsiung P, Ko TH, Hartl I, Fujimoto JG. 2003. High-resolution optical coherence microscopy for high-speed, in vivo, cellular imaging. Opt Lett 28:2064–2066.

Barton JK, Guzman F, Tumlinson AR. 2004. Dual modality instrument for simultaneous optical coherence tomography imaging and fluorescence spectroscopy. J Biomed Opt 9:618–623.

Beaurepaire E, Moreaux L, Amblard F, Mertz J. 1999. Combined scanning optical coherence and two-photon-excited fluorescence microscopy. Opt Lett 24:969–971.

Breuls RG, Mol A, Petterson R, Oomens CWJ, Baaijens FPT, Bouten CVC. 2003. Monitoring local cell viability in engineered tissues: A fast, quantitative, and nondestructive approach. Tissue Eng 9:269–281.

Constantinidis I, Stabler CL, Long R, Jr, Sambanis A. 2002. Noninvasive monitoring of a retrievable bioartificial pancreas in vivo. Ann N Y Acad Sci 961:298–301.

Curtis A, Riehle M. 2001. Tissue engineering: The biophysical background. Phys Med Biol 46:47–65.

Denk W, Strickler JH, Webb WW. 1990. Two-photon laser scanning fluorescence microscopy. Science 248:73–76.

Desai T. 2000. Micro- and nanoscale structures for tissue engineering constructs. Med Eng Phys 22:595–606.

Dunkers JP, Cicerone MT, Washburn NR. 2003. Collinear optical coherence and confocal fluorescence microscopies for tissue engineering. Opt Express 11:3074–3079.

Gareau DS, Bargo PR, Horton WA, Jacques SL. 2004. Confocal fluorescence spectroscopy of subcutaneous cartilage expressing green fluorescent protein versus cutaneous collagen autofluorescence. J Biomed Opt 9:254–258.

Griffith L. 2002. Emerging design principle in biomaterials and scaffolds for tissue engineering. Ann N Y Acad Sci 969:83–95.

Huang D, Swanson EA, Lin CP, Schuman JS, Stinson WG, Chang W, Hee MR, Flotte T, Gregory K, Puliafito CA, Fujimoto JG. 1991. Optical coherence tomography. Science 254:1178–1181.

Izatt J, Hee MR, Owen G, Swanson EA, Fujimoto JG. 1994. Optical coherence microscopy in scattering media. Opt Lett 19:590–592.

Leitgeb RA, Wojtkowski M, Kowalczyk A, Hitzenberger CK, Sticker M, Fercher AF. 2000. Spectral measurement of absorption by spectroscopic frequency-domain optical coherence tomography. Opt Lett 25:820–822.

Leitgeb RA, Hitzenberger CK, Fercher AF. 2003. Performance of Fourier-domain vs. time-domain optical coherence tomography. Opt Express 11:889–894.

Lin ASP, Barrows TH, Cartmella SH, Guldberg RE. 2003. Microarchitectural and mechanical characterization of oriented porous polymer scaffolds. Biomaterials 24:481–489.

Lippincott-Schwartz J, Patterson GH. 2003. Development and use of fluorescent protein markers in living cells. Science 300:87–91.

Morgner U, Drexler W, Kartner FX, Li XD, Pitris C, Ippen EP, Fujimoto JG. 2000. Spectroscopic optical coherence tomography. Opt Lett 25:111–113.

Norman JJ, Desai TA. 2005. Control of cellular organization in three dimensions using a microfabricated polydimethylsiloxane-collagen composite tissue scaffold. Tissue Eng 11:378–386.

Rubart M. 2004. Two-photon microscopy of cells and tissues. Circ Res 95:1154–1166.

Stephens DJ, Allan VJ. 2003. Light microscopy techniques for live cell imaging. Science 300:82–86.

Stevens MM, George JH. 2005. Exploring and engineering the cell surface interface. Science 310:1135–1138.

Tan W, Sendemir-Urkmez A, Fahrner LJ, Jamison R, Leckband D, Boppart SA. 2004. Structural and functional optical imaging of

three-dimensional engineered tissue development. Tissue Eng 10: 1747–1756.
Tan W, Oldenburg AL, Norman JJ, Desai TA, Boppart SA. 2006. Optical coherence tomography of cell dynamics in three-dimensional tissue models. Opt Express 14:7159–7171.
Tang S, Krasieva TB, Chen Z, Tromberg BJ. 2006. Combined multiphoton microscopy and optical coherence tomography using a 12-fs broadband source. J Biomed Opt 11:020502.
Tsien RYT. 1998. The green fluorescent protein. Annu Rev Biochem 67:509–544.
Xu C, Ye J, Marks DL, Boppart SA. 2004. Near-infrared dyes as contrast-enhancing agents for spectroscopic optical coherence tomography. Opt Lett 29:1647–1649.
Xu C, Vinegoni C, Ralston TS, Luo W, Tan W, Boppart SA. 2006. Spectroscopic spectral-domain optical coherence microscopy. Opt Lett 31:1079–1081.
Vinegoni C, Ralston TS, Tan W, Luo W, Marks DL, Boppart SA. 2006. Integrated structural and functional optical imaging combining spectral-domain optical coherence and multiphoton microscopy. Appl Phys Lett 88:053901.